



# Femtosecond laser inscribed helical long period fiber grating for exciting orbital angular momentum

JIAYAN CHEN,<sup>1,2</sup> ZHIYONG BAI,<sup>1,2,\*</sup>  GUOXUAN ZHU,<sup>1,2</sup> RUI LIU,<sup>1,2</sup> CHUROU HUANG,<sup>1,2</sup> ZHENG HUANG,<sup>1,2</sup> LUPING WU,<sup>1,2</sup> CHANGRUI LIAO,<sup>1,2</sup>  AND YIPING WANG<sup>1,2</sup>

<sup>1</sup>Key Laboratory of Optoelectronic Devices and Systems of Ministry of Education/Guangdong Province, College of Physics and Optoelectronic Engineering, Shenzhen University, Shenzhen 518060, China

<sup>2</sup>Shenzhen Key Laboratory of Photonic Devices and Sensing Systems for Internet of Things, Guangdong and Hong Kong Joint Research Centre for Optical Fibre Sensors, Shenzhen University, Shenzhen 518060, China  
\*baizhiyong@szu.edu.cn

**Abstract:** A method employing femtosecond lasers to inscribe helical long period fiber grating (HLPPFG) for exciting orbital angular momentum (OAM) of light is experimentally demonstrated. In this method, the refractive index modulation (RIM) of HLPPFG is realized by three-dimensional translation of a fiber without rotation, indicating better stability, repeatability and flexibility. The coupling efficiency can be customized by varying the radius of the helical RIM, except laser energy. The characteristics of phase and polarization purity of the coupled modes in HLPPFGs are studied. Results show that HLPPFGs can directly excite OAM modes, the polarization state and helical phase of the mode can be adjusted independently, and the purity is the highest at resonant wavelength, over 91%.

© 2022 Optica Publishing Group under the terms of the [Optica Open Access Publishing Agreement](#)

## 1. Introduction

In 1992, Allen et al. recognized that optical beams with a helical phase carrying orbital angular momentum (OAM) and the helical phase wavefront can be described as  $\exp(il\varphi)$ , where  $\varphi$  is the azimuthal angle and  $l$  is the topological charge [1]. Due to unique characteristics of orthogonality and phase singularity, OAM beams have been applied in optical communications [2], microscopic imaging [3], optical tweezers [4], and so on. In these applications, the generation and control of OAM beams is the key technology to be studied. Because of the compactness, low cost, long-distance transmission and compatibility with the optical fiber communication system, the fiber-based OAM generation technology has attracted intensive attention. Thus far, many OAM beam generators based on optical fiber devices have been proposed and implemented, including writing or printing holograms on the end face of the fiber [5], off-axis incidence of light [6], few-mode fiber couplers [7], fiber Bragg gratings [8], long period fiber grating (LPFG) [9–14] and so on [15,16]. OAM beams generators based on LPFGs have the advantages of low loss, high coupling and wavelength selectivity, but some auxiliary accessories are required, such as polarization controller, pressure plate, and fiber rotator [9–13]. Helical long period fiber grating (HLPPFG) possesses all of the superiorities belonging to LPFGs, and can directly excite the spiral phase without any auxiliary accessories, indicating better stability, flexibility and integration in potential applications.

At present, there are two main methods to inscribe HLPPFG. One is to twist hot-melt fiber [17–23] into a spiral deformation under a high-temperature condition. In this method, the high stability of the fabrication system and the uniform heating of the silicon are strictly required to ensure that the heated fibers are uniformly twisted during fabrication, which is a major obstacle to obtaining high-quality gratings. The other is to focus the CO<sub>2</sub> laser beam on the optical fiber

which simultaneously translates along the optical fiber axis and rotates around the optical fiber axis to form helical refractive index modulation. The optical fiber is not twisted, which reduced the requirements for heating and twisting optical fiber, so it is easier to get high-quality HLPFG [24]. However, this method still needs to rotate the optical fiber and the requirements for coaxial and synchronization of the optical fiber rotator are still high. At the same time, the size of the laser spot limits the preparation of small pitch HLPFG and the thermal radiation effect of laser will damage the structure of optical fiber. It is well known that femtosecond laser can induce optical modification limited to the focusing center area on the fiber substrate, so as to realize refractive index modulation in small areas [25–27]. Thus, the helical grating modulation can be directly achieved by changing the relative position between the laser focus and the fiber which is moved by three-dimension translation stages with a spiral path. The method does not involve fiber rotation, and has better flexibility, stability and ease of realization.

In this paper, HLPFGs were prepared by focusing the femtosecond laser beam into an optical fiber moved along a spiral path realized by using the three-dimensional translation stages. Since the fiber rotation was not involved, the fabrication processing possesses a better stability, which was proved by inscribing a series of HLPFG samples with different grating pitches. The HLPFGs with different spiral radius were achieved from  $0.5\mu\text{m}$  to  $7.5\mu\text{m}$  at an interval of  $1\mu\text{m}$ , and the results show that the highest coupling efficiency was obtained when the radius was  $4.5\mu\text{m}$  which located at the interface between fiber core and cladding. The intensity distribution and phase of the coupled modes in these HLPFGs were investigated experimentally, as a result, the Laguerre-Gaussian-like beams were obtained with radial exponent of 2, which have three-layer ring structure in intensity and helical wavefront in phase. The purity and polarization characteristics were studied as well. Results show that, the mode purity of HLPFGs was over 91% near the resonant wavelength for incident light with arbitrary polarization state. When the operated wavelength deviates from the resonant wavelength, the purity of OAM mode decreases. Moreover, the excitation of the helical phase and its mode purity in HLPFGs are independent of the polarization state of the input light.

## 2. HLPFG fabrication and spectral characteristics

A femtosecond laser (PHAROS,  $513\text{nm}/290\text{fs}/200\text{kHz}$ ) was used to fabricate the HLPFG, schematically shown in Fig. 1(a). In order to prepare HLPFG with strong coupling efficiency and high quality, it is necessary to select an appropriate objective to obtain a focused spot with a suitable size. In the experiment, the laser is focused using a 20x objective with a numerical aperture of 0.4 to obtain a laser spot with an area of approximately  $2\mu\text{m}^2$ , and the fabrication process of HLPFG was monitored by a CCD. The optical fiber used in this work is single mode fiber (SMF) with a core and cladding diameter of  $9\mu\text{m}$  and  $125\mu\text{m}$ , respectively. In experiment, the fabrication of HLPFG mainly involves the following steps. First, a section of SMF is fixed on the 3D translation stages with the fiber axis paralleling to the X-axis. Then, the spiral path was selected for the fiber with a designed spiral radius and pitch. Finally, the laser spot is focused on the fiber core, and the fiber is simultaneously moved along the spiral path driven by the 3D translation stages, thereby forming a spiral refractive index modulation belonging to HLPFG. Meanwhile, the HLPFG transmission spectrum was monitored using an optical spectrum analyzer (OSA) assisted by a broadband spontaneous emission light source.

In order to verify the reliability of the fabrication method, a series of HLPFGs with pitches of  $515\mu\text{m}$ ,  $520\mu\text{m}$ ,  $525\mu\text{m}$  and  $530\mu\text{m}$  were fabricated, and the laser average power, spiral radius and periods number were  $10.78\text{mW}$ ,  $4.5\mu\text{m}$ , and 20, respectively. Figure 1(b) shows the transmission spectrum for these HLPFGs. It can be seen from Fig. 1(b) that under the same processing parameters, the coupling strength of the four gratings are similar. In addition, the resonant wavelength redshifts with the increase of the grating pitches and this change trend is consistent

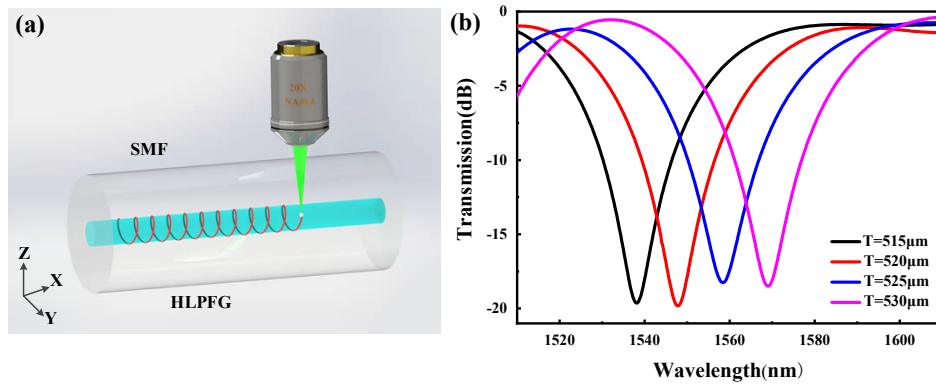


**Fig. 1.** (a) Schematic diagram of HLPFG inscription with a femtosecond laser; (b) transmission spectrum of the HLPFGs with pitches of 515 $\mu\text{m}$ , 520 $\mu\text{m}$ , 525 $\mu\text{m}$  and 530 $\mu\text{m}$ .

with that of LPFG. The above characteristics show that the proposed preparation method for HLPFG is reliable.

The HLPFGs with different spiral radius was fabricated from 0.5 to 7.5 $\mu\text{m}$  with an interval of 1 $\mu\text{m}$ , to investigate the evolution of mode coupling efficiency. The grating pitch and average power to fabricate these HLPFGs was 530 $\mu\text{m}$  and 10.78mW, respectively. The appropriate periods number were chosen to achieve similar resonance depths for these samples. Under the same conditions, the fewer periods number required, the higher the coupling efficiency of HLPFG. Figure 2 shows the transmission spectrum of these HLPFGs with the periods number of 85,44,27,22,19,20,27 and 30 corresponding to the different spiral radius, respectively. With the increase of spiral radius, the number of periods decreases first and then increases. The minimum number of periods required occurs at a spiral radius of 4.5 $\mu\text{m}$ . When the spiral radius is far away from 4.5 $\mu\text{m}$ , the number of periods increases, that is, the grating length required to achieve similar coupling strength increases, which indicates that the coupling efficiency decreases. When the spiral radius is 0.5 $\mu\text{m}$ , the coupling strength is only 9.2dB under the maximum grating length

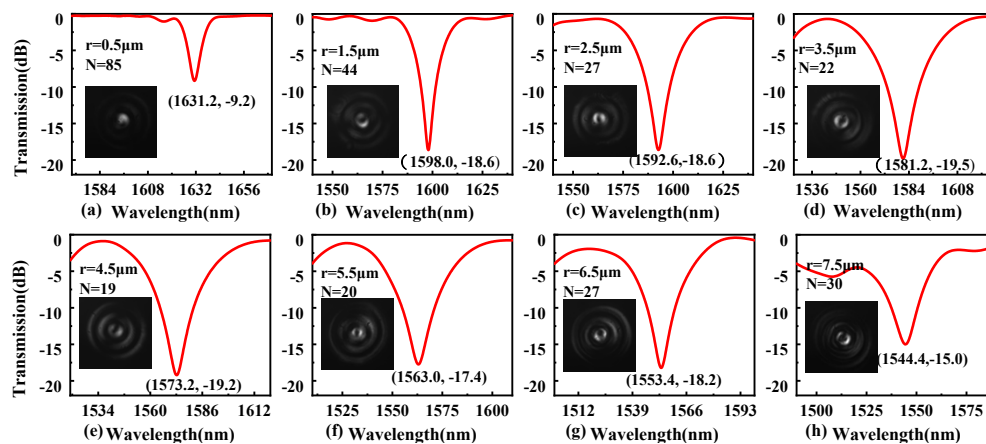


**Fig. 2.** Transmission spectrum of the HLPFGs with radius of (a) 0.5 $\mu\text{m}$ , (b) 1.5 $\mu\text{m}$ , (c) 2.5 $\mu\text{m}$ , (d) 3.5 $\mu\text{m}$ , (e) 4.5 $\mu\text{m}$ , (f) 5.5 $\mu\text{m}$ , (g) 6.5 $\mu\text{m}$  and (h) 7.5 $\mu\text{m}$ , respectively. The average power of the sample preparation process and the pitch were 10.78mW, 530 $\mu\text{m}$ , respectively.

allowed by the preparation system, showing a low coupling efficiency. When the spiral radius is  $7.5\mu\text{m}$ , the grating is over coupled at 15.0dB, showing a low mode coupling efficiency and a large background loss. Therefore, when the spiral radius is close to the interface between the core and the cladding, the coupling efficiency is the highest. In addition, the resonant wavelength of the HLPFG shifts blue with the increase of the spiral radius. This may be due to the change of self-coupling coefficient in the phase matching condition of HLPFG. With the increase of helical RIM radius, the distribution of grating modulation intensity in the spatial position of core and cladding changes, resulting in the self-coupling coefficient decrease in fiber core and the increase in fiber cladding, as a such, the resonant wavelength is blue-shift [28].

The clockwise HLPFG (C-HLPFG) and anticlockwise HLPFG (A-HLPFG) were fabricated to investigate the mode coupling characteristics. The average power, spiral radius, pitch and periods number were 10.78mW,  $4.5\mu\text{m}$ ,  $530\mu\text{m}$  and 20, respectively. The microscopic image of C-HLPFG and A-HLPFG were respectively shown in Fig. 3(a) and (b). The resonant wavelength and dip loss of the C-HLPFG and A-HLPFG were 1570.6nm, 18.7dB and 1573.2nm, 19.2dB, respectively. The coupling strength of the two HLPFGs was over 98%.

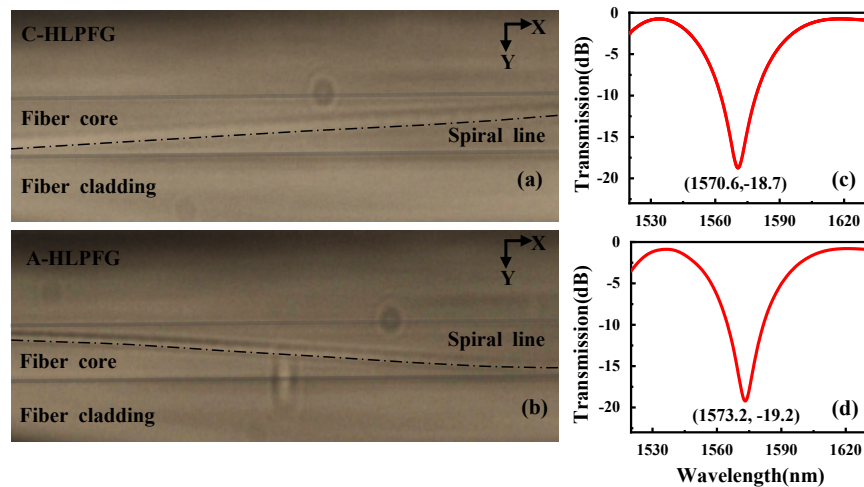


**Fig. 3.** Microscopy image of the inscribed (a) C-HLPFG, and (b) A-HLPFG, and transmission spectra of (c) C-HLPFG, and (d) A-HLPFG.

### 3. Mode coupling characteristics

The mode intensity distribution and phase excited in HLPFG were investigated by using experiment setup in Fig. 4(a). A beam of light from a tunable laser was divided into two paths by a beam splitter. A path of light was injected into the HLPFG to excite the OAM modes. The other path of light, as the reference beam, interferes with the generated OAM modes at a beam combiner to verify the excitation of spiral phase. When the reference light was blocked and all of the polarizers and wave-plates were absent, the intensity distributions of coupled mode in HLPFGs were observed and recorded by a CCD, which were shown in Fig. 4(b) and (c). Because the gratings were written in SMF and the coupled OAM modes belong to cladding mode which cannot be transmitted over a long distance, the intensity distribution of coupled modes were observed from fiber end about 2mm away from the HLPFG. Results show that, the coupled mode in HLPFGs, has a three-layer ring structure in intensity distribution, which is similar to that of the first-order Laguerre Gaussian beam with a radial index of 2. Further, we verify the phase of the coupled mode by coaxial interference method. In order to avoid the inconvenience of

observation and analysis caused by multi-layer interference, we used an aperture to make only the innermost ring interfere with the reference light. As shown in Fig. 4(d) and (e), the spiral interference patterns with a single topological charge were obtained. It is proved that the -1- and +1-order OAM modes are excited in the C-HLPFG and A-HLPFG, respectively. Thus, it is verified experimentally that HLPFG inscribed by femtosecond laser can directly excite OAM mode as well.

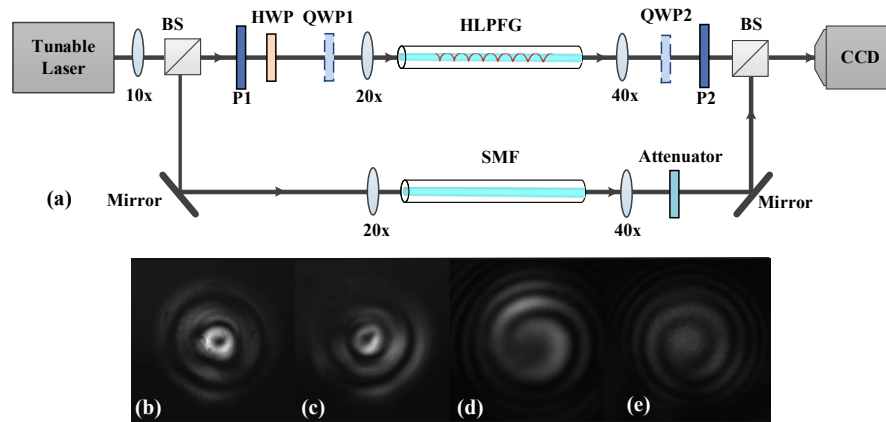


**Fig. 4.** (a) Experimental setup for studying intensity distribution and phase of the coupled mode in HLPFGs; the mode intensity distribution of coupled mode in (b) C-HLPFG and (c) A-HLPFG; interference patterns between reference beam and the innermost rings of the coupled mode for (d) C-HLPFG and (e) A-HLPFG. HWP, half-wave plate; QWP1, quarter-wave plate 1; QWP2, quarter-wave plate 2; P1, polarizer 1; P2, polarizer 2.

By changing the polarization states of the input fundamental mode and detecting that of the output light from HLPFG, the polarization characteristics of the coupled OAM modes was investigated. The change and detection of the polarization states were achieved by the combination of polarizer and wave plates inserted in the experimental setup shown in Fig. 4(a) with the reference path of light was blocked. In the experiment, the input fundamental mode was modulated into linearly and circularly polarized light respectively, and then tested the polarization states of OAM mode. Figure 5(a) presents the measured results for C-HLPFG, and the specific experiments are as follows. First, the linearly polarized input light purified by polarizer (P1), which was marked as  $LP^{\parallel}$ , was directly incident into HLPFG. The polarization state of the output OAM modes from HLPFG was tested by a polarizer (P2). The polarization direction of P2 was marked as ‘ $\uparrow$ ’, ‘ $\rightarrow$ ’, ‘ $\downarrow$ ’, ‘ $\leftarrow$ ’. With the rotation of P2, the output OAM intensity appears periodic extinction, as shown in the first line of Fig. 5(a), indicated that the polarization state of the generated OAM beam is linear as well. Second, by inserting and rotating a half wave plate (HWP1) in experiment setup, the linearly polarized input light marked as  $LP^{\perp}$  which was perpendicular to  $LP^{\parallel}$  was obtained, and then was incident into HLPFG. The measurement results as shown in the second line of Fig. 5(a), show that the excited OAM modes possessed a linearly polarized state which is similar to that of the input fundamental mode.

Then replace HWP1 with a quarter wave plate (QWP1) to obtain circular polarized light. QWP1 was rotated to obtain left-handed and right-handed circularly polarized input light and marked them as LCP and RCP, respectively. The intensity of the obtained OAM modes kept constant when P2 was rotated. Thus, a quarter wave plate (QWP2) was used and inserted between the HLPFG sample and P2. The measured results for the LCP and RCP were recorded in the third and fourth line of Fig. 5(a), which indicated that, the coupled OAM modes were LCP and RCP,

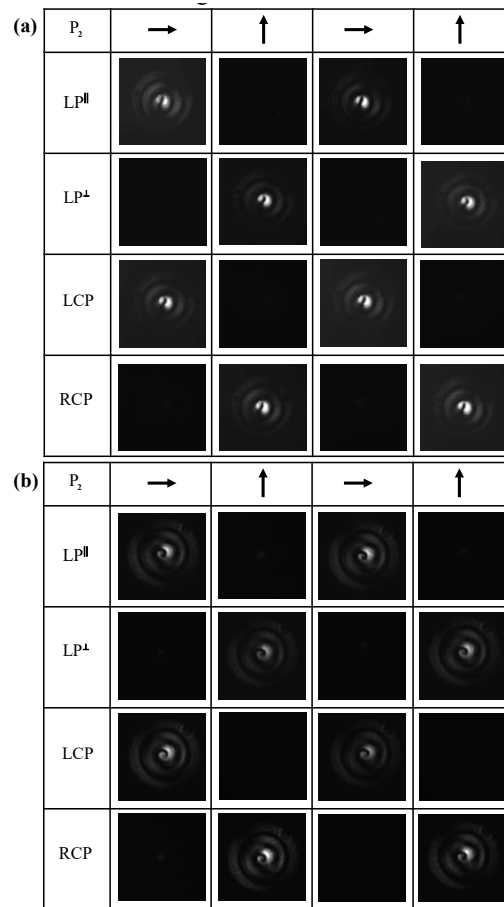
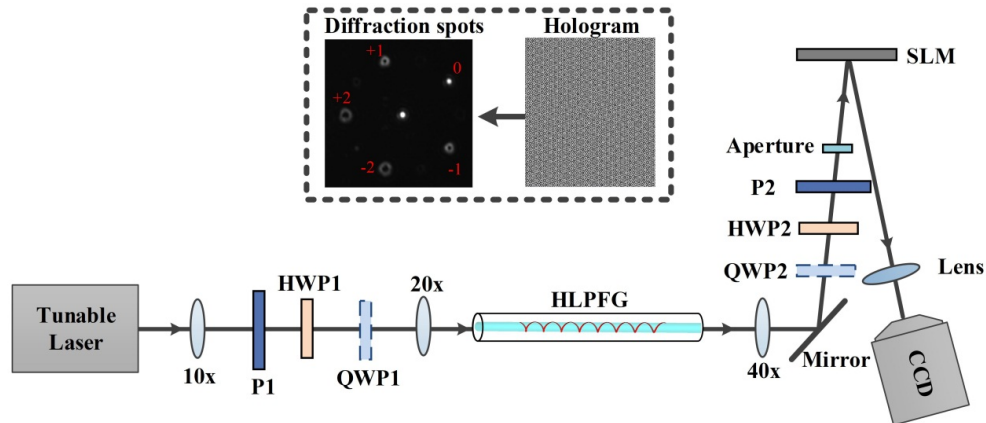


**Fig. 5.** The intensity changes of the coupled OAM modes with respect to different polarization state of input light. The polarization characteristics measured results of (a) C-HLPPFG and (b) A-HLPPFG.

respectively, corresponding to the polarization state of input light. Figure 5(b) is the experimental results of A-HLPPFG, which is the same as that of C-HLPPFG. The experimental results show that the inscribed HPLPPFGs excite OAM beam with the same polarization state as that of the incident light.

The purity of the resulting OAM modes is a key issue for its practical application, which was measured by using mode decomposition method, and the experiment setups were schematically shown in Fig. 6(a). The OAM beam generated from the HPLPPFG sample was incident on a spatial light modulation (SLM) and then was reflected into CCD. A Daman grating was loaded on the SLM to divide the input beam into six beams with the same light intensity. The six beams were arranged in a pentagonal pattern. Thereof, the beam in the center position was not modulated and kept consistent with features of the input light. The other five beams were respectively added a phase modulation of  $-2$ ,  $-1$ ,  $0$ ,  $+1$ ,  $+2$ . When a Gaussian beam is incident onto the SLM, the five outer beams are modulated to OAM modes with the order of  $-2$ ,  $-1$ ,  $0$ ,  $+1$ , and  $+2$  respectively. When the OAM beam generated by HPLPPFG sample is incident onto the SLM, the outer beams which contained the conjugated phase will be converted to a Gaussian beam. Therefore, the contribution of each component of the OAM mode was measured by recording the power at

the center of the converted modes. In order to observe the influence of different polarization states on the mode purity of OAM beam at the same time, and to ensure the parallel between the polarization direction of input light and response direction of SLM, polarizers and wave plates are added to the optical path, as is shown in Fig. 6(a).



(b)

	$LP^{\parallel}$	$LP^{\perp}$	LCP	RCP
C-HLPFG				
A-HLPFG				

**Fig. 6.** (a) Experimental setups and (b) results for measuring the purity of OAM mode excited by HLPFG. P1, polarizer 1; P2, polarizer 2; HWP1, half-wave plate1; HWP2, half-wave plate2; QWP1, quarter-wave plate1; QWP2, quarter-wave plate2; SLM, spatial light modulator.

In experiment, the purity of OAM modes excited by the HLPFG was measured when the light with  $LP^{\parallel}$ ,  $LP^{\perp}$ , LCP, and RCP states were input. The results are shown in Fig. 6(b). The order of OAM mode generated by C-HLPFG and A-HLPFG are -1 and +1, respectively, and is consistent under input light with different polarized states, that is, the polarization states of input light do not affect the generation and topological charge number of the OAM modes in HLPFGs. The power ratio between the different component of OAM modes was calculated to determine the purity. As seen in Fig. 7(a)-(d) for C-HLPFG and 7(e)-(h) for A-HLPFG, the purity of  $\pm 1^{\text{st}}$ -order OAM mode was over 91% near the resonant wavelength for incident light with arbitrary polarization state. Therefore, the excitation of the helical phase in HLPFGs is independent of the polarization state of the input light. At the same time, we measured the change of OAM mode purity within

10nm bandwidth at an interval of 0.2nm. As shown in Fig. 7, as the test wavelength deviates from the resonant wavelength, the purity of OAM mode decreases and the proportion of other mode components increases accordingly. For the C-HLPPFG and A-HLPPFG, the OAM mode purity respectively are over 86% and 88% within 2nm bandwidth, over 74% and 80% within 4nm bandwidth, and over 42% and 49% within the 10nm bandwidth. This evolution characteristic is related to the bandwidth and coupling strength of the HLPPFGs themselves. Therefore, a required OAM mode converter can be realized by appropriately designing the grating parameters.

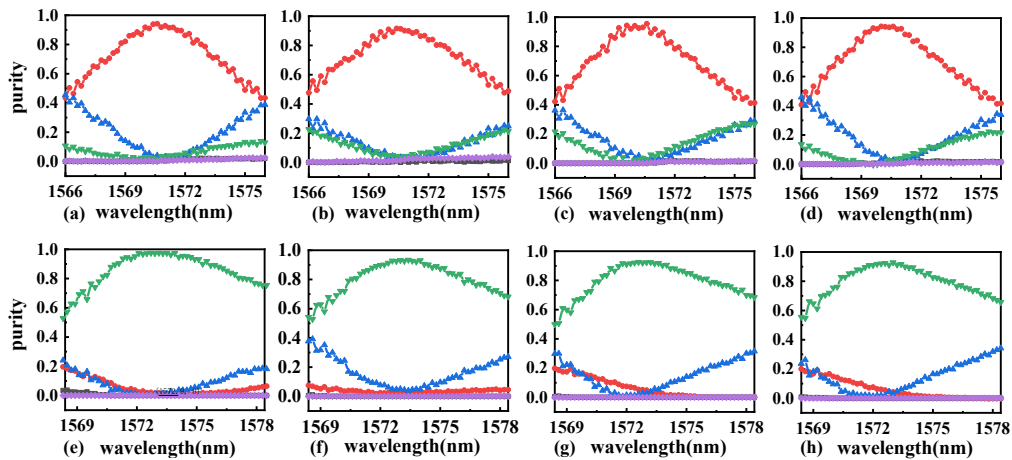


**Fig. 7.** OAM mode purity evolving with different input wavelengths and polarization states of incident light. Purity of OAM mode with  $l=-1$  excited in A-HLPPFG under input light with (a)  $LP^{\parallel}$ , (b)  $LP^{\perp}$ , (c) LCP and (d) RCP polarization states. Purity of OAM mode with  $l=+1$  excited in C-HLPPFG under input light with (e)  $LP^{\parallel}$ , (f)  $LP^{\perp}$ , (g) LCP and (h) RCP polarization states. The black, red, blue, green and purple lines represent -2, -1, 0, +1, +2 order OAM, respectively.

#### 4. Conclusion

A method with strong stability, good repeatability and high flexibility for preparing HLPPFG has been experimentally researched and verified. In this method, a new modulation parameter, the radius of the spiral path, is introduced, which provides a new degree of freedom for the preparation and application of HLPPFG. This method can be applied to optical fibers that better support OAM mode transmission, such as few-mode fiber, ring core fiber and so on. In addition, this method can be used to fabricate helical fiber Bragg gratings by choosing a suitable objective and adjusting grating period. At the same time, the experimental results of mode characteristics show that the HLPPFG can directly excite the helical phase and the excitation of the helical phase is independent of the polarization state of the input light. In addition, the purity of OAM modes decreases as the test wavelength deviates from the resonance wavelength, which can be optimized by designing a wide bandwidth and high coupling strength HLPPFG.

**Funding.** National Natural Science Foundation of China (61875134, 61905155, 62005169); Shenzhen Science and Technology Innovation Program (JCYJ20180507182058432); Shenzhen University (2019097).

**Disclosures.** The authors declare no conflicts of interest.

**Data availability.** Data underlying the results presented in this paper are not publicly available at this time but may be obtained from the authors upon reasonable request.

## References

1. L. Allen, M. W. Beijersbergen, R. J. C. Spreeuw, and J. P. Woerdman, "Orbital angular momentum of light and transformation of Laguerre Gaussian Laser modes," *Phys. Rev. A* **45**(11), 8185–8189 (1992).
2. N. Bozinovic, Y. Yue, Y. X. Ren, M. Tur, P. Kristensen, H. Huang, A. E. Willner, and S. Ramachandran, "Terabit-scale orbital angular momentum mode division multiplexing in fibers," *Science* **340**(6140), 1545–1548 (2013).
3. N. Bokor and Y. Iketaki, "Laguerre-Gaussian radial Hilbert transform for edge-enhancement Fourier transform x-ray microscopy," *Opt. Express* **17**(7), 5533–5539 (2009).
4. Y. Han and D. G. Grier, "Fluid dynamics: Vortex rings in a constant electric field," *Nature* **424**(6946), 267–268 (2003).
5. P. Vayalankuzhi, S. Bhattacharya, U. Eigenthaler, K. Keskinbora, C. T. Sاملan, M. Hirscher, J. P. Spatz, and N. K. Viswanathan, "Direct patterning of vortex generators on a fiber tip using a focused ion beam," *Opt. Lett.* **41**(10), 2133–2136 (2016).
6. X. Q. Jin, F. F. Pang, Y. Zhang, S. J. Huang, Y. C. Li, J. X. Wen, Z. Y. Chen, M. Wang, and T. Y. Wang, "Generation of the First-Order OAM Modes in Single-Ring Fibers by Offset Splicing Technology," *IEEE Photonics Technol. Lett.* **28**(14), 1581–1584 (2016).
7. Y. Yan, J. Wang, L. Zhang, J. Y. Yang, I. M. Fazal, N. Ahmed, B. Shamee, A. E. Willner, K. Birnbaum, and S. Dolinar, "Fiber coupler for generating orbital angular momentum modes," *Opt. Lett.* **36**(21), 4269–4271 (2011).
8. X. Q. Zhang, A. T. Wang, R. S. Chen, Y. Zhou, H. Ming, and Q. W. Zhan, "Generation and conversion of higher order optical vortices in optical fiber with helical fiber bragg gratings," *J. Lightwave Technol.* **34**(10), 2413–2418 (2016).
9. Y. H. Zhao, Y. Q. Liu, L. Zhang, C. Y. Zhang, J. X. Wen, and T. Y. Wang, "Mode converter based on the long-period fiber gratings written in the two-mode fiber," *Opt. Express* **24**(6), 6186–6195 (2016).
10. H. Zhao and H. P. Li, "Advances on Mode-Coupling Theories, Fabrication Techniques, and Applications of the Helical Long-Period Fiber Gratings: A Review," *Photonics* **8**(4), 106 (2021).
11. W. D. Zhang, K. Y. Wei, L. G. Huang, D. Mao, B. Q. Jiang, F. Gao, G. Q. Zhang, T. Mei, and J. L. Zhao, "Optical vortex generation with wavelength tunability based on an acoustically-induced fiber grating," *Opt. Express* **24**(17), 19278–19285 (2016).
12. H. Wu, S. C. Gao, B. S. Huang, Y. H. Feng, X. C. Huang, W. P. Liu, and Z. H. Li, "All-fiber second-order optical vortex generation based on strong modulated long-period grating in a four-mode fiber," *Opt. Lett.* **42**(24), 5210–5213 (2017).
13. S. H. Li, Q. Mo, X. Hu, C. Du, and J. Wang, "Controllable all-fiber orbital angular momentum mode converter," *Opt. Lett.* **40**(18), 4376–4379 (2015).
14. C. N. Alexeyev and M. A. Yavorsky, "Generation and conversion of optical vortices in long-period helical core optical fibers," *Phys. Rev. A* **78**(4), 043828 (2008).
15. M. Yavorsky, D. Vikulin, C. Alexeyev, and V. Belotelov, "Photon-phonon spin-orbit interaction in optical fibers," *Optica* **8**(5), 638–641 (2021).
16. M. Bernas, K. Zolnacz, M. Napiorkowski, G. Statkiewicz-Barabach, and W. Urbanczyk, "Conversion of LP<sub>11</sub> modes to vortex modes in a gradually twisted highly birefringent optical fiber," *Opt. Lett.* **46**(18), 4446 (2021).
17. X. M. Xi, G. K. L. Wong, M. H. Frosz, F. Babic, G. Ahmed, X. Jiang, T. G. Euser, and P. S. J. Russell, "Orbital-angular-momentum-preserving helical Bloch modes in twisted photonic crystal fiber," *Optica* **1**(3), 165–169 (2014).
18. Y. Zhang, Z. Y. Bai, C. L. Fu, S. Liu, J. Tang, J. Yu, C. R. Liao, Y. Wang, J. He, and Y. P. Wang, "Polarization-independent orbital angular momentum generator based on a chiral fiber grating," *Opt. Lett.* **44**(1), 61–64 (2019).
19. C. L. Fu, Y. P. Wang, Z. Y. Bai, S. Liu, Y. Zhang, and Z. L. Li, "Twist-direction-dependent orbital angular momentum generator based on inflation-assisted helical photonic crystal fiber," *Opt. Lett.* **44**(2), 459–462 (2019).
20. C. L. Fu, S. Liu, Z. Y. Bai, J. He, C. R. Liao, Y. Wang, Z. L. Li, Y. Zhang, K. M. Yang, B. Yu, and Y. P. Wang, "Orbital angular momentum mode converter based on helical long period fiber grating inscribed by hydrogen-oxygen flame," *J. Lightwave Technol.* **36**(9), 1683–1688 (2018).
21. L. Zhang, Y. Q. Liu, Y. H. Zhao, and T. Y. Wang, "High sensitivity twist sensor based on helical long-period grating written in two-mode fiber," *IEEE Photonics Technol. Lett.* **28**(15), 1629–1632 (2016).
22. G. K. L. Wong, M. S. Kang, H. W. Lee, F. Biancalana, C. Conti, T. Weiss, and P. S. J. Russell, "Excitation of orbital angular momentum resonances in helically twisted photonic crystal fiber," *Science* **337**(6093), 446–449 (2012).
23. C. L. Fu, S. Liu, Y. Wang, Z. Y. Bai, J. He, C. R. Liao, Y. Zhang, F. Zhang, B. Yu, S. C. Gao, Z. H. Li, and Y. P. Wang, "High-order orbital angular momentum mode generator based on twisted photonic crystal fiber," *Opt. Lett.* **43**(8), 1786–1789 (2018).
24. Z. Y. Bai, Y. P. Wang, Y. Zhang, C. L. Fu, S. Liu, M. Q. Li, C. R. Liao, Y. Wang, and J. He, "Helical Long-Period Fiber Gratings as Wavelength-Tunable Orbital Angular Momentum Mode Generators," *IEEE Photonics Technol. Lett.* **32**(7), 418–421 (2020).
25. J. W. Chan, T. R. Huser, S. H. Risbud, J. S. Hayden, and D. M. Krol, "Waveguide fabrication in phosphate glasses using femtosecond laser pulses," *Appl. Phys. Lett.* **82**(15), 2371–2373 (2003).
26. Z. M. Zheng, Y. S. Yu, X. Y. Zhang, Q. Guo, and H. B. Sun, "Femtosecond Laser Inscribed Small-Period Long-Period Fiber Gratings with Dual-Parameter Sensing," *IEEE Sensors J.* **18**(3), 1100–1103 (2018).
27. J. He, B. J. Xu, X. Z. Xu, C. R. Liao, and Y. P. Wang, "Review of Femtosecond-Laser-Inscribed Fiber Bragg Gratings: Fabrication Technologies and Sensing Applications," *Photonic Sens.* **11**(2), 203–226 (2021).

28. T. Erdogan, "Fiber grating spectra," *J. Lightwave Technol.* **15**(8), 1277–1294 (1997).